

Spin injection and electric field effect in degenerate semiconductors

Irene D'Amico

*Istituto Nazionale per la Fisica della Materia (INFM);
Institute for Scientific Interchange, via Settimio Severo 65, I-10133 Torino, Italy*

(Dated: May 25, 2020)

We analyze spin-transport in semiconductors in the regime characterized by $T \lesssim T_F$ (intermediate to degenerate), where T_F is the Fermi temperature. Such a regime is of great importance since it includes the lightly doped semiconductor structures used in most experiments; we demonstrate that, at the same time, it corresponds to the regime in which carrier-carrier interactions assume a relevant role. Starting from a general formulation of the drift-diffusion equations, which includes many-body correlation effects, we perform detailed calculations of the spin injection characteristics of various heterostructures, and analyze the combined effects of carrier density variation, applied electric field and Coulomb interaction. We show the existence of a *degenerate* regime, peculiar to semiconductors, which strongly differs, as spin-transport is concerned, from the degenerate regime of metals.

PACS numbers: 72.25.-b, 72.10.-d, 72.25.Dc

I. INTRODUCTION

Despite many efforts and some substantial progress, major difficulties persist in the practical implementation of semiconductor spintronics devices. One of the fundamental problems inherent the electrical injection of spin currents into semiconductors is the so-called conductivity mismatch¹: the large conductivity difference between metals and semiconductors induces a spin accumulation at the interface which in turn drastically reduces spin injection into the semiconductor.

Recently Yu and Flatté (YF)² have pointed out the possibility of improving the efficiency of spin injection through the application of a strong, but experimentally accessible, electric field. At variance with metals, in semiconductors, this field remains partially unscreened so that it is necessary to explicitly introduce a drift-related term in the spin-transport equations.

The YF analysis of the semiconductor high-field regime neglects electron-electron interaction effects – aside from those responsible for macroscopic charge neutrality – and, perhaps more importantly, focuses on the high-field *non-degenerate* regime (see Eq. (1)), especially insofar as the analysis of heterostructures are concerned.

In the present paper we extend and refine their analysis in several directions. Starting from a more general formulation of the drift-diffusion equations, which includes many-body correlation effects, we perform detailed calculations of the spin injection characteristics of various heterostructures.

First of all we perform a careful analysis of the regime to which GaAs and ZnSe-based structures (most commonly used in spintronics experiments) belong. We point out that, with the exception of lightly doped samples at *room temperature*, these systems are generally in a regime which cannot be described by non-degenerate electron statistics. In particular, the low temperature heterostructures used in Refs.3 and 4 are in the degenerate regime (see Fig. 1). We then study these structures

under the effect of an applied electric field and introduce the “semiconductor degenerate regime” characterized by the inequalities $k_B T \ll \varepsilon_F \ll e|E|L_s$, where ε_F is the Fermi energy of the carriers in the semiconductor and E is the applied electric field. This high-field regime occurs, for comparable materials and doping densities, at fields which are one order of magnitude smaller than in the non-degenerate high-field regime. In particular, the use of non-degenerate statistics in heterostructures based on GaAs, ZnSe or comparable materials, at a few Kelvin, can overestimate the effect of the electric field by orders of magnitude (see Sec.IV).

As for Coulomb interactions, we demonstrate that the experimentally relevant regime corresponds to the one in which the many body effects are at their strongest. Neglecting these effects can induce both quantitative as well as qualitative errors. Coulomb interactions affect the system through the spin Coulomb drag effect^{5,6,7} and by reducing the longitudinal spin stiffness. In particular we will discuss how the spin drag explicitly modifies spin-transport whenever materials with different magnetic properties are joined.

The numerical part of this paper concentrates on sandwiched structures (ferromagnet (FM)/non-magnetic semiconductor (NMS)/ferromagnet) which are of the utmost importance in device applications based on the magnetoresistance effect. We have performed a detailed analysis of the spatial dependence of various quantities such as electrochemical potentials, density and current polarizations for both parallel and antiparallel alignment of the ferromagnets. At variance with the parallel case, we find that in the antiparallel case, the magnetoresistance can be *increased* by a strong electric field.

Another important issue we address is the effect of the dependence of the spin diffusion constant D_s on carrier density when $k_B T \lesssim \varepsilon_F$ (see inset of Fig. 1). We will show that, due to this dependence, it is possible to greatly enhance the local spin current density by carefully choosing the system parameters.

This paper is organized as follows: in Sec. II we discuss the system regimes as doping density, temperature, and electric field are varied; in Sec. III we derive the drift-diffusion equation for spin-transport including both the Coulomb interaction and the electric field, and discuss the behavior of the upstream and downstream diffusion lengths; in Sec. IV we discuss the limits of the non-degenerate approximation; in Sec. V we consider the spin current and the implications of varying the carrier density on this quantity; in Sections VI and VII we analyze FM/NMS and FM/NMS/FM heterostructures, respectively; in Sec. VIII we describe the effects of Coulomb interactions; finally in Sec. IX we draw our main conclusions. Two appendices, discussing some details of the proposed heterostructure-related formalism and proposing “exact” equations for describing spin transport in non-interacting degenerate heterostructures conclude the paper.

II. DOPING DENSITY, TEMPERATURE AND ELECTRIC FIELD -RELATED REGIMES

This work focuses on electrically driven spin transport: due to the presence of the external electric field, the system is characterized by *three different energy scales* whose relative magnitude determines the system behavior. Such energies are the Fermi energy $\varepsilon_F = \hbar^2 k_F^2 / 2m$ (which strongly depends on the carrier density), the thermal energy $k_B T$ and the energy related to the electric field $e|E|L_s$, where $L_s = \sqrt{D_s \tau_s}$ is the diffusion length, D_s the diffusion constant and τ_s the spin-flip time.

Let us first of all define the regimes the system undergoes depending on the relation between thermal and Fermi energies

$$k_B T \gg \varepsilon_F \text{ non-degenerate regime} \quad (1)$$

$$k_B T \ll \varepsilon_F \text{ degenerate regime} \quad (2)$$

$$k_B T \approx \varepsilon_F \text{ intermediate regime.} \quad (3)$$

The intermediate regime corresponds to the crossover region between the first two, roughly the region between the dotted lines in Fig. 1.

We will concentrate our discussion on NMS in the *intermediate and degenerate* regimes. Such regimes are of utmost importance since they include most of the semiconductor structures used in spintronics related experiments, such as n-doped GaAs³ or Zn_{0.97}Be_{0.03}Se⁴ ones. This is illustrated in Fig. 1, where we plot the ratio $k_B T / \varepsilon_F$ as a function of the carrier density n for n-doped GaAs (upper panel) and (Zn,Be)Se (lower panel). Three different values of the temperature are considered (as labelled). The regions corresponding to degenerate and non-degenerate systems are specified as well. As can be seen, up to room temperatures, for densities as low as $n \sim 5 \cdot 10^{16} \text{ cm}^{-3}$ in GaAs or $n \sim 10^{18} \text{ cm}^{-3}$ in (Zn,Be)Se the system is at most in the intermediate regime; for $T = 1.6 \text{ K}$, a temperature often used in experiments, the

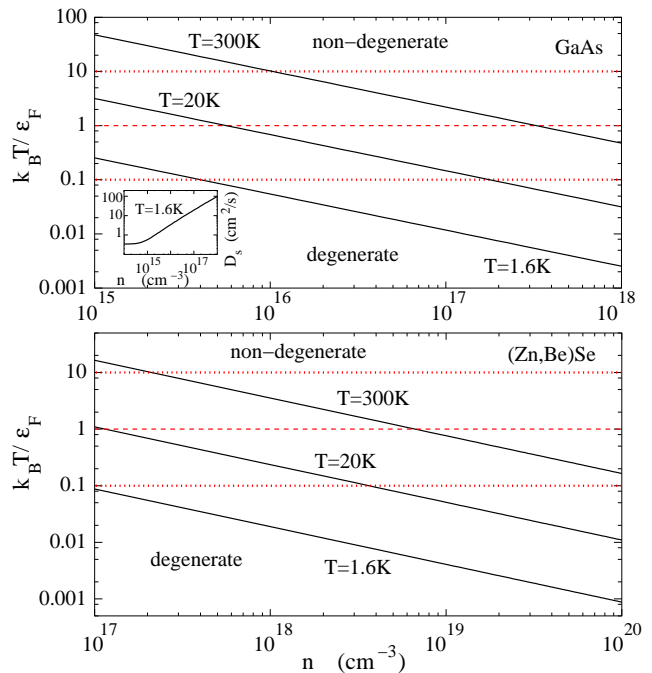


FIG. 1: $k_B T / \varepsilon_F$ vs carrier density n for GaAs (upper panel, $m = 0.067m_0$, $\epsilon = 12$) and (Zn, Be)Se (lower panel, $m = 0.5m_0$, $\epsilon = 12$) parameters, at $T = 1.6 \text{ K}$, 20 K , 300 K , as labelled. Degenerate and non-degenerate regions are indicated as well. Inset: D_s vs carrier density for $T = 1.6 \text{ K}$ and GaAs parameters.

system remains in the *degenerate* regime for the whole relevant density range.

Since, as just discussed, in most experimental situations $k_B T \lesssim \varepsilon_F$, the other relevant information to determine the expected system behavior is contained in the ratio $e|E|L_s / \varepsilon_F$.

In Fig. 2 we plot this ratio as a function of density and for fields up to 1000 V/cm , for both GaAs and (Zn,Be)Se. In both cases we have chosen $L_s = 2 \mu\text{m}$. We will consider this same value in all the calculations presented¹³. The high ($e|E|L_s \gg \varepsilon_F$) and low ($e|E|L_s \ll \varepsilon_F$) field regions are explicitly indicated. We notice that, even at very low densities, it is necessary to apply fields of the order of 100 V/cm to enter the high field regime.

As we will explain in detail, the comparison of the energy scales, as done in Fig. 1 and Fig. 2, is a very efficient way to understand in which regime the considered system is and deduce how and if the electric field is going to affect the diffusion lengths and the spin-transport related quantities. In particular *at variance with metals*, in semiconductors the Fermi energy can be so low that, even for moderate electric fields, we can fulfill the condition $e|E|L_s \gg \varepsilon_F \gg k_B T$. This is what we define as “semiconductor degenerate regime” to distinguish it from the well-know “metallic” degenerate regime in which $\varepsilon_F \gg e|E|L_s$ for any reasonable field. In the “semi-

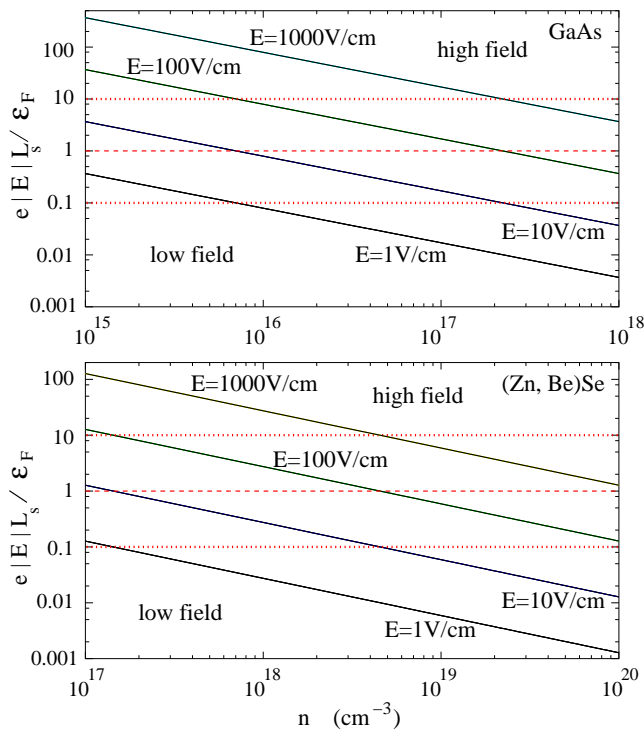


FIG. 2: $e|E|L_s/\varepsilon_F$ vs carrier density n for GaAs (upper panel) and (Zn, Be)Se (lower panel) parameters, for $E = 1, 10, 100, 1000$ V/cm as labelled. High and low field regions are indicated as well.

conductor degenerate regime” the electric field heavily affects spin-transport even if the system is degenerate. In order to illustrate this point, we will analyze in detail the behavior of the penetration lengths L_d and L_u as electric field and carrier density change.

Due to its importance, in this article we will mainly discuss n-doped GaAs at $T = 1.6$ K; our results are based on the interplay among different energy scales, so that they can be readily extended to other semiconductor materials.

III. INTERACTING DRIFT-DIFFUSION EQUATION

First of all we will sketch the derivation of the general drift-diffusion equation for spin-transport which *includes Coulomb interactions* among carriers. We refer the reader to Ref. 7 for the details.

We start from the drift diffusion equation for the interacting spin- α charge current

$$\vec{j}_\alpha(\vec{r}) = \sum_\beta \left(\sigma_{\alpha\beta} \vec{E} + e D_{\alpha\beta} \vec{\nabla} n_\beta \right), \quad (4)$$

where $\sigma_{\alpha\beta}$ is the (*non-diagonal*) homogeneous conductivity matrix of the electron gas and $D_{\alpha\beta}$ is the (*non-*

diagonal) diffusion matrix. Throughout the paper Greek indices will correspond to the spin-variables \uparrow, \downarrow . We substitute Eq. (4) in the generalized continuity equation for the spin-density components

$$\frac{\partial \Delta n_\alpha(\vec{r}, t)}{\partial t} = -\frac{\Delta n_\alpha(\vec{r}, t)}{\tau_{sf,\alpha}} + \frac{\Delta n_{\bar{\alpha}}(\vec{r}, t)}{\tau_{sf,\bar{\alpha}}} + \frac{\vec{\nabla} \cdot \vec{j}_\alpha(\vec{r})}{e}, \quad (5)$$

where $\Delta n_\alpha(\vec{r}, t) \equiv n_\alpha(\vec{r}, t) - n_\alpha^{(0)}$, $n_\alpha(\vec{r}, t)$ is the α density component, $n_\alpha^{(0)}$ its equilibrium value and $\tau_{sf,\alpha}$ is the α spin-flip relaxation time. Carefully applying⁷ the local charge neutrality constraint

$$\Delta n_\uparrow(r) = -\Delta n_\downarrow(r) \quad (6)$$

and considering the regime linear in ∇n_α , the general interacting drift-diffusion equation is obtained⁷.

Finally, imposing the steady state condition $\partial(\Delta n_\uparrow - \Delta n_\downarrow)/\partial t = 0$ we obtain the steady-state *interacting* drift-diffusion equation

$$-\frac{(\Delta n_\uparrow - \Delta n_\downarrow)}{\tau_s} + D_s \nabla^2 (\Delta n_\uparrow - \Delta n_\downarrow) + \mu_s \vec{E} \cdot \vec{\nabla} (\Delta n_\uparrow - \Delta n_\downarrow) = 0, \quad (7)$$

where $\tau_s = (1/\tau_{sf,\uparrow} + 1/\tau_{sf,\downarrow})^{-1}$ is the spin relaxation time, and the effective interacting mobility and diffusion constants are given, for a non-magnetic system⁸, by

$$\mu_s = e\tau_D/m \quad (8)$$

and

$$D_s = \frac{\mu_s S n}{e} \frac{1}{1 - \rho_{\uparrow\downarrow}/\rho_D}. \quad (9)$$

Here $\rho_D = m/ne^2\tau_D$ is the ordinary Drude resistivity, m the effective mass of the carriers, S the (interacting) static longitudinal spin-stiffness⁷, $n = n_\uparrow + n_\downarrow$ the carrier density and $\rho_{\uparrow\downarrow}$ the spin-transresistivity, which measures the momentum rate exchanged between spin up and spin down carriers^{5,6,7}. Eq. (7) is valid independently of the value of $k_B T/\varepsilon_F$.

If the sample is homogeneous and $\vec{E} \parallel \hat{x}$ the solution to Eq. (7) is given by

$$\Delta n_\uparrow - \Delta n_\downarrow = A e^{x/L_u} + B e^{-x/L_d} \quad (10)$$

with A, B determined by the boundary conditions and

$$L_{u,d}^{-1} = \pm \frac{\mu_s |E|}{2D_s} + \sqrt{\left(\frac{\mu_s |E|}{2D_s} \right)^2 + \frac{1}{D_s \tau_s}}. \quad (11)$$

$L_{u,d}$ are the *interacting* upstream and downstream “penetration” lengths¹². Such quantities correspond to the average decay lengths of an injected spin-unbalance in the upstream (L_u) and downstream (L_d) directions.

The upper panel of Fig. 3 shows the behavior of L_d , as a function of density for GaAs at $T=1.6$ K and

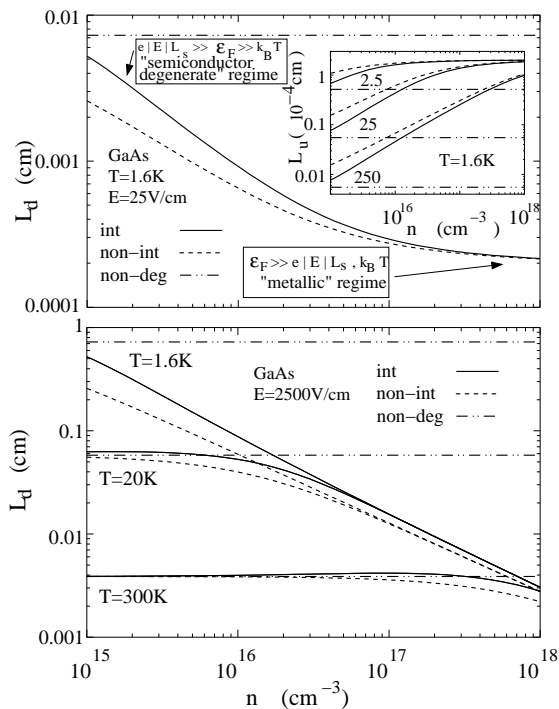


FIG. 3: Upper panel: downstream diffusion length L_d vs carrier density for GaAs parameters, $T=1.6\text{K}$ and $E=25\text{V/cm}$. Solid line refers to the interacting calculation, dashed line to the non-interacting approximation and dashed-double dotted line to the non-degenerate limit. Inset: Upstream diffusion length L_u vs density n for GaAs parameters at $T = 1.6\text{K}$ and three different fields (as labelled in V/cm units). Line types as in the main panel. Lower panel: downstream diffusion length L_d vs carrier density for GaAs parameters, $T=1.6\text{K}$, 20K and 300K (as labelled) and $E=2500\text{V/cm}$. Line types as in the upper panel.

$E = 25\text{V/cm}$. The solid line represents the fully interacting calculation, the dashed one the non-interacting approximation and the dashed double dot line the non-degenerate limit obtained by setting $D_s = \mu_s k_B T / e$ in Eq. (11). In this, and in all the following calculations, we have set $\mu_s = 3 \times 10^3 \text{cm}^2/\text{Vs}$.³ However we stress that, at least in the degenerate regime, for which usually $\rho_{\uparrow\downarrow}/\rho_D \ll 1$, $L_{u,d}$ is basically independent from μ_s (see Eqs. (11) and (9)).

Let us focus on the crossovers undergone by the system when the carrier density is increased. At this temperature even at very low densities the system is degenerate ($\varepsilon_F \gg k_B T$), so the interesting interplay is between the Fermi energy and the electric field related energy: as shown in the figure, depending on the system density, the Fermi energy can be low enough to enter, even for moderate electric fields, the “semiconductor degenerate regime” $e|E|L_s \gg \varepsilon_F$. The existence of such a regime implies that, *even for a degenerate system*, the drift term in Eq. (7) cannot be neglected, i.e. it is not possible to describe spin-transport using a diffusion equation for the

electrochemical potentials, as usually done for metals¹⁴. Even in *degenerate* semiconductor systems in fact, the drift term severely modifies the penetration lengths $L_{u,d}$, varying their values over order of magnitudes (as clearly shown for L_d in Fig. 3). As a rule of thumb, we see that in this regime the order of magnitude of such a variation is set by the ratio $e|E|L_s/\varepsilon_F$. The “semiconductor degenerate” regime extends to higher densities when the applied field is increased. Notice that, even in this regime, the actual value of L_d strongly differs from its non-degenerate limit. By increasing the carrier density, the system will eventually enter the “metallic” regime (as indicated in the figure), in which the drift term can be neglected and $L_{u,d}$ recover their unperturbed value L_s .

Similar results, i.e. order of magnitude variations depending on the carrier density and quantitative importance of Coulomb interactions are obtained for the upstream penetration length L_u (see upper inset), with the key difference that in the “semiconductor degenerate regime” L_u is strongly *reduced* by the electric field effect, being the product $L_u \cdot L_d = L_s$ constant¹³.

It is interesting to ask what happens in the high field regime $e|E|L_s \gg (\varepsilon_F, k_B T)$ when both temperature and carrier density varies. In Fig. 3, lower panel, we plot L_d in the high field regime ($E=2500\text{V/cm}$), as a function of carrier density and for three different temperatures, $T = 1.6\text{K}$, $T = 20\text{K}$ and $T = 300\text{K}$. In addition to the crossovers discussed in relation to the upper panel, for low densities and $T = 300\text{K}$ the system enters the non-degenerate regime $\varepsilon_F \ll k_B T$ (see also Fig. 1). In this region in fact, the non-degenerate approximation coincides with the interacting calculation. Fig. 3 shows that the greatest variations due to the presence of the electric field are actually reached by lowering the temperature and for any reasonable density and the materials considered, correspond to the “semiconductor degenerate” regime.

IV. LIMITS OF THE NON-DEGENERATE APPROXIMATION

As demonstrated in Sec. II, the use of non-degenerate electron statistics to describe carrier dynamics in commonly-used semiconductors is justified only for very lightly doped semiconductors at high temperatures. For this reason, when analyzing spin transport, particular care must be taken in determining the correct system regime: for some other problems an easy-to-implement approximation, used outside its supposed validity regime, can still yield reasonable estimates⁹; unfortunately this is not the case for the non-degenerate approximation in semiconductor spin-transport. It is tempting, since it leads to simpler analytical formulas, to approximate D_s in the various quantities (from the penetration lengths to the spin current, from the injected density polarization to the magnetoresistance), by its non-degenerate, classical expression. Unfortunately as it has been ex-

perimentally shown³ and theoretically confirmed¹¹, the spin diffusion constant varies over *orders of magnitude* going from the non-degenerate to the intermediate and degenerate regime (see inset of Fig. 1, in which D_s is plotted as a function of n for GaAs parameters). This implies that approximating spin transport behavior by non-degenerate expressions in the wrong regime can lead to quite large errors. In Fig. 3, Fig. 4 and Fig. 10 we have compared the interacting calculation (solid line) with its non-degenerate approximation (dashed double-dot line) for some of the most relevant quantities, as penetration lengths, spin current, and magnetoresistance respectively. At low temperatures, even for densities as low as $n \sim 5 \times 10^{16} \text{cm}^{-3}$ and fields as small as $E=10 \text{V/cm}$ (low-field regime), this approximation can overestimate the field effect by *orders of magnitude*. Such a discrepancy is quite general and is found also for quantities such as injected density and current polarizations (not shown).

V. THE SPIN CURRENT

We will now focus on the spin-current in a non-magnetic system. Starting from the drift-diffusion Eq. (4), and imposing the conditions $D_s = D_{\uparrow\uparrow} - D_{\uparrow\downarrow} = D_{\downarrow\downarrow} - D_{\downarrow\uparrow}$ and $\mu_s = \mu_{\uparrow\uparrow} + \mu_{\uparrow\downarrow} = \mu_{\downarrow\downarrow} + \mu_{\downarrow\uparrow}$ which are obtained from the general formula for D_s and μ_s ⁷ in the non-magnetic limit and in the regime linear in ∇n_α , the charge current becomes

$$\vec{j}(\vec{r}) := j_\uparrow(\vec{r}) + j_\downarrow(\vec{r}) = e\vec{E}\mu_s(n_\uparrow + n_\downarrow) \quad (12)$$

while the spin current assumes the form:

$$\vec{j}_s(\vec{r}) := j_\uparrow(\vec{r}) - j_\downarrow(\vec{r}) = \vec{j}P(x) + eD_s n \nabla P(x) \quad (13)$$

with $P(x) = (n_\uparrow - n_\downarrow)/n$ the density polarization. If we consider a spin unbalance injected at $x = 0$, i.e. such that in Eq. (10) either $A = 0$ ($x > 0$) or $B = 0$ ($x < 0$), $\Delta n_\uparrow - \Delta n_\downarrow$ will acquire a simple exponential form; the upstream ($x < 0$) (downstream ($x > 0$)) spin current will then be given by

$$\vec{j}_s^{u,d}(\vec{r}) = \left[\vec{j} \mp (-e) \frac{nD_s}{L_{u,d}} \hat{x} \right] P(x) = (\vec{j} + \vec{j}_D^{u,d})P(x). \quad (14)$$

Eq. (14) is very interesting because it clearly shows how the spin current is composed: $\vec{j}_s^{u,d}$ results in fact as the sum of two distinct parts, the first corresponding to the *total* drift current \vec{j} and the second being a *total* diffusion current \vec{j}_D . Both the components are “weighted” by $P(x)$, the percentage of spin-polarized carriers. It is interesting to notice that in the downstream case, $\vec{j} \parallel \vec{j}_D$, so that both diffusion and drift phenomena positively contribute to the spin-current, while in the upstream case \vec{j} and \vec{j}_D are in competition. It is easy to see that in the limit of very large electric fields, $1/L_d \rightarrow 0$ so that $\vec{j}_s^d(\vec{r}) = \vec{j}P(x)$, while $1/L_u \rightarrow |E|\mu_s/D_s$ and $\vec{j}_s^u(\vec{r})$ exactly vanishes. Keeping in mind that the diffusion constant increases by orders of magnitude when going from

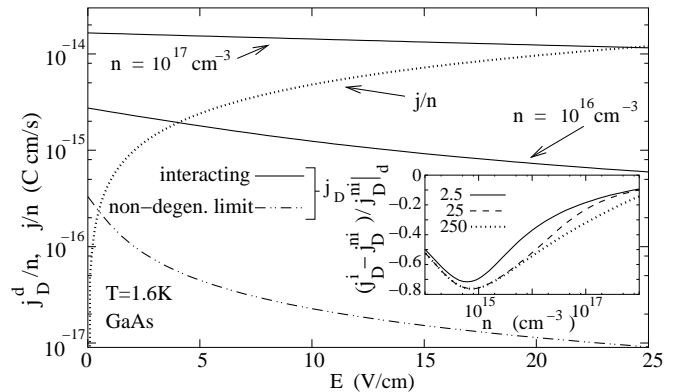


FIG. 4: Diffusion current density j_D and total current density j (rescaled by total carrier density n) vs electric field E in the downstream direction for GaAs parameters, $T=1.6\text{K}$ and two different carrier densities (as labelled). Solid lines refer to the interacting j_D/n , and the dashed-double-dot line to the non-degenerate limit of j_D/n . Dotted line refers to j/n . Inset: correction to the non-interacting approximation $(j_D^d - j_D^{nl})/j_D^{nl}$ vs carrier density for $E = 2.5, 25, 250 \text{V/cm}$.

the non-degenerate to the degenerate regime, Eq. (14) suggests that a method to increment the spin current for a given electric field should be to enter the degenerate regime (for example by lowering the temperature), increasing in this way the diffusive part of the current. If instead the doping (or the temperature) is kept constant, an increase in the electric field will increase the drift current \vec{j} . In this last case though, $1/L_d$ will decrease, and to the incremented \vec{j} will correspond a decreasing of \vec{j}_D .

We illustrate this behavior in Fig. 4. In this figure we plot j_D^d and j at $T = 1.6\text{K}$ rescaled by the trivial (and common) dependence on the carrier density n as a function of the applied electric field and for two different densities (as indicated). j/n (dotted curve) does not depend on the density nor on Coulomb interaction. The fully interacting j_D^d/n corresponds to the solid line. If we fix the density and increase the electric field, j_D decreases and j increases; but if we fix the electric field (considering a moderate electric field), and increase the density, j_D increases while j does not change, so that there is no competition between the two quantities. We underline once more that this is not due to a trivial linear scaling with the carrier density, but to the behavior of the diffusion constant when entering the degenerate regime. Regarding $P(x)$, the second factor in Eq. (14), if we consider as injector a not-fully polarized metal in the degenerate regime and for moderate fields, we can easily deduce from Eq. (32) (next session), that $P(0) \sim n^{1/3}$, i.e. $P(x)$ slightly increases with carrier density. This implies that in such a regime our conclusions hold for the full spin current j_s^d .

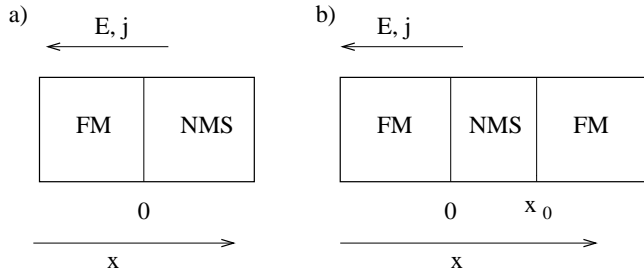


FIG. 5: Schematic view of the FM/NMS (left) and FM/NMS/FM (right) heterostructures considered.

VI. FM/NMS JUNCTION

We will now concentrate on FM/NMS heterostructures. The schematic view of the system is illustrated in Fig. 5a. We will first derive explicit expressions for the quantities of interest (electrochemical potential, density and current polarization, magnetoresistance, etc) in the interacting case, for *general* carrier density n and temperature T and then concentrate on the degenerate regime. As underlined before, this regime is experimentally relevant, and, as discussed in detail in Sec. VII, in it Coulomb interactions are quantitatively important.

In the *non-interacting* approximation it is possible to write explicit expressions for the chemical potential in both the non-degenerate and degenerate regime. By using them, the equations for the quantities of interest can be derived (see respectively Ref. 2 and Appendix B). Since we want to derive instead equations which include Coulomb interactions and are valid independently from the doping regime, let us consider the Taylor expansion of the interacting chemical potential

$$\mu_{\sigma}^{\text{chem}}(n_{\uparrow}, n_{\downarrow}) = \mu_{0\sigma}^{\text{chem}} + \frac{\partial \mu_{\sigma}^{\text{chem}}}{\partial n_{\sigma}} \Delta n_{\sigma} + \frac{\partial \mu_{\sigma}^{\text{chem}}}{\partial n_{\bar{\sigma}}} \Delta n_{\bar{\sigma}} + \dots \quad (15)$$

If we use the relation

$$S_{\sigma\delta} \equiv \frac{\partial \mu_{\sigma}^{\text{chem}}}{\partial n_{\delta}} \quad (16)$$

between the $\{\sigma\delta\}$ element of the spin-stiffness tensor and the chemical potential, and the local charge neutrality constraint Eq. (6), we can rewrite such a potential as

$$\mu_{\sigma}^{\text{chem}} \approx \mu_{0\sigma}^{\text{chem}} + (S_{\sigma\sigma} - S_{\sigma\bar{\sigma}}) \Delta n_{\sigma}. \quad (17)$$

The limits of this approximation are discussed in Appendix A. The excess electrochemical potential associated to Eq. (17) then becomes

$$\Delta \mu_{\sigma} \equiv \mu_{\sigma} - \mu_{0\sigma}^{\text{chem}} \quad (18)$$

$$\approx (S_{\sigma\sigma} - S_{\sigma\bar{\sigma}}) \Delta n_{\sigma} + e \vec{E} \cdot \vec{x} + B. \quad (19)$$

Eq. (19) is general and is valid both for polarized and non-magnetic materials.

By using the relation between the spin stiffness and the spin stiffness tensor components

$$S = (S_{\uparrow\uparrow} - S_{\uparrow\downarrow} + S_{\downarrow\downarrow} - S_{\downarrow\uparrow})/4, \quad (20)$$

the symmetries in the NMS ($S_{\uparrow\uparrow} - S_{\uparrow\downarrow} = S_{\downarrow\downarrow} - S_{\downarrow\uparrow}$), and the local charge neutrality constraint, the electrochemical potential in the NMS ($x > 0$) is given by

$$\begin{aligned} \Delta \mu_{\uparrow(\downarrow)} &= \pm S n P(x) + e \vec{E} \cdot \vec{x} + B \\ &= \pm \frac{D_s e}{\mu_s} (1 - \rho_{\uparrow\downarrow}/\rho_D) P(x) + e \vec{E} \cdot \vec{x} + B \end{aligned} \quad (21)$$

where the plus (minus) sign refers to the \uparrow (\downarrow) spin component and we have used Eq. (9) in the second expression.

If we assume that the FM (diluted magnetic semiconductor or metal) is in the “metallic” degenerate regime (as it is often the case), the electrochemical potential on the FM side ($x < 0$) will be^{2,16}

$$\begin{pmatrix} \Delta \mu_{\uparrow} \\ \Delta \mu_{\downarrow} \end{pmatrix} = e \frac{\vec{j} \cdot \vec{x}}{\sigma^f} \begin{pmatrix} 1 \\ 1 \end{pmatrix} + C e \vec{j} \cdot \hat{x} \begin{pmatrix} 1/\sigma_{\uparrow}^f \\ -1/\sigma_{\downarrow}^f \end{pmatrix} \exp\left(\frac{x}{L_f}\right) \quad (22)$$

In this expression Coulomb interactions are included through $\sigma_{\sigma}^f \equiv \sigma_{\sigma\sigma}^f + \sigma_{\sigma\bar{\sigma}}^f$ ¹⁶. Since in this regime the spin transresistivity is much smaller than the Drude resistivity⁵, we will neglect the former in our calculations.

If we assume transparent interfaces, the boundary conditions to be satisfied at $x = 0$ will be

$$j_s|_{0-} = j_s|_{0+} \quad (23)$$

$$\Delta \mu_{\uparrow}|_{0-} = \Delta \mu_{\uparrow}|_{0+} \quad (24)$$

$$\Delta \mu_{\downarrow}|_{0-} = \Delta \mu_{\downarrow}|_{0+}. \quad (25)$$

The spin current components are given by

$$e \vec{j}_{\sigma} = \sum_{\delta} \sigma_{\sigma\delta} \frac{\partial \Delta \mu_{\delta}}{\partial x} \hat{x}, \quad (26)$$

and the spin currents in the two materials will then become

$$\vec{j}_s^f = \vec{j} \left(p_f + \frac{2C}{L_f} \exp\left(\frac{x}{L_f}\right) \right) \quad (27)$$

$$\vec{j}_s^{sc} = P(x) (\vec{j} + \vec{j}_D^d) \quad (28)$$

where the indexes f , sc correspond respectively to the FM and to the NMS, $p_f \equiv (\sigma_{\uparrow}^f - \sigma_{\downarrow}^f)/(\sigma_{\uparrow}^f + \sigma_{\downarrow}^f)$ and \vec{j}_D^d is defined by Eq. (14).

By using Eqs. (21)-(28), after some straightforward algebra, we derive the expressions for the quantities of interest.

The electrochemical potential in the NMS will be

$$\Delta \mu_{\uparrow(\downarrow)} = -S n P(0) [p_f \mp \exp(-x/L_d)] + e \vec{E} \cdot \vec{x}, \quad (29)$$

where the - (+) sign refers to the \uparrow (\downarrow) spin component. In particular the expression for the interface band splitting is given by

$$\Delta \mu_{\uparrow}(0) - \Delta \mu_{\downarrow}(0) = 2S n P(0) \stackrel{E \rightarrow \infty}{=} 2S n p_f \quad (30)$$

We see that the splitting saturates for high electric fields. The relation $Sn = D_s e(1 - \rho_{\uparrow\downarrow}/\rho_D)/\mu_s$ implies on the other hand that this limit can be increased by increasing the diffusion constant D_s (for example by increasing the system density as previously discussed).

The magnetoresistance (which is related to the electrochemical potential sum at the interface and will be discussed in detail later) can be written as

$$R_m = -\frac{\Delta\mu_{\uparrow}(0) + \Delta\mu_{\downarrow}(0)}{2e|j|} = \frac{SnP(0)p_f}{e|j|}. \quad (31)$$

The equation for the injected density polarization is

$$P(0) = L_u \left(\frac{1}{L_u} - \frac{1}{L_d} \right) \frac{p_f}{\frac{\sigma_f}{\sigma_{sc}} \frac{(1-p_f^2)}{L_f} L_u (1 - \rho_{\uparrow\downarrow}/\rho_D) + 1} \quad (32)$$

while the one for the injected current polarization is

$$\alpha(0) = \frac{p_f}{\frac{\sigma_f}{\sigma_{sc}} \frac{(1-p_f^2)}{L_f} L_u (1 - \rho_{\uparrow\downarrow}/\rho_D) + 1}, \quad (33)$$

where we have used the relations $E\mu_s/D_s = (1/L_u - 1/L_d)$. We stress that Eqs. (29)-(33) are valid in all density and field regimes and represent the fully interacting expressions.

Fig. 6 illustrates the behavior of the \uparrow and \downarrow electrochemical potentials (excluding the trivial linear dependence on x , as we will do in all figures related to such quantities) as a function of x across the FM/NMS junction and for increasing field and FM polarization. The parameters used in the calculations we present are $n = 5.2 \cdot 10^{16} \text{cm}^{-3}$ ($\varepsilon_F = 7.6 \text{meV}$), $\sigma^f/\sigma_{sc} = 95$, $L_f = 20 \text{nm}$, $L_s = 2 \mu\text{m}^{13}$. In the upper panel of Fig. 6 the FM polarization is $p_f = 0.5$. As the figure shows, the splitting of the FM sub-bands at the interface increases asymmetrically in respect to their asymptotic values (at $-\infty$), with the electric field due to the difference between the conductivities σ_{\uparrow}^f , σ_{\downarrow}^f . In the inset we plot the same electrochemical potentials but on the NMS side of the junction ($x > 0$). As expected the potentials are now symmetric with respect to their asymptotic value (at ∞) and the extension of the spin-polarized region in which $\nabla\mu_{\sigma} \neq \text{const}$ extends in space as the electric field increases. As can be seen, the potential drop at the interface (the difference between the values of the electrochemical potentials at $\pm\infty$), which is related to the magnetoresistance, increases with the field.

The lower panel of Fig. 6 illustrates the influence of increasing the FM polarization on the electrochemical potentials at the junction and in the high field regime ($E = 1000 \text{V/cm}$). Fig. 7 shows in detail the behavior of the related quantities as p_f is increased from 0.5 to full polarization. While most of the considered quantities (from the injected current and density polarizations to the sub-band splitting to the magnetoresistance) monotonically increase with the FM polarization to saturate when $p_f = 1$, the \uparrow sub-band split (dashed line labelled

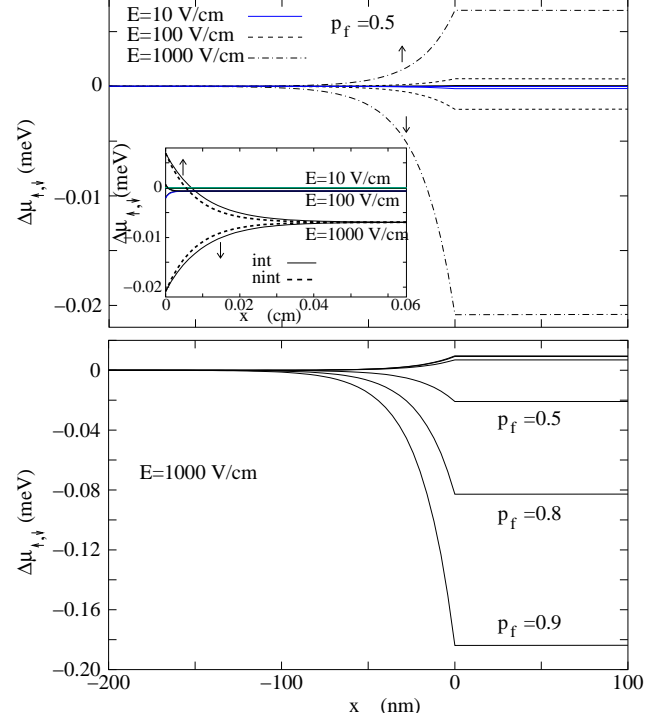


FIG. 6: Upper panel: Up and down electrochemical potentials (without the term linear in x) at the junction vs x for three different fields (as labelled) and $p_f = 0.5$. Inset: as in main panel but on the NMS side of the junction. The non-interacting approximation (dashed line) is plotted as well. Lower panel: As in the upper panel but for three different FM polarizations (as labelled) and $E = 1000 \text{V/cm}$.

with \uparrow) increases at first to rapidly drop to zero when the FM polarization saturates.

As in non-degenerate systems², P_0 saturates towards the α_0 value as the field increases (not shown).

A. Magnetoresistance

A very important quantity for building “on-off” type devices as magnetic field sensors or read heads for magnetic hard disk drives¹⁷ is the so called magnetoresistance R_m . It can be defined as the part of the equivalent resistance R_{eq} of the device which depends on its magnetic properties.

For the considered structure R_{eq} is given by

$$R_{eq} \equiv -\frac{\Delta\mu(\lambda_{sc}) - \Delta\mu(-\lambda_f)}{e|j|}, \quad (34)$$

where $\lambda_{sc(f)}$ are the device lengths in the NMS and FM regions, and $\Delta\mu = (\Delta\mu_{\uparrow} + \Delta\mu_{\downarrow})/2$ indicates the variation of the electrochemical potential with respect to the situation in which no electric field is applied, and no junction is present. We will define R_m as R_{eq} minus the trivial,

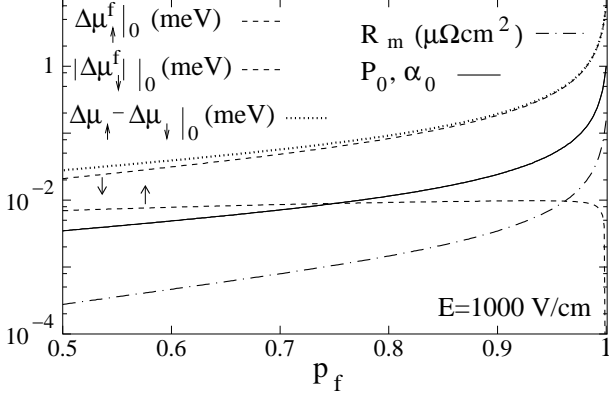


FIG. 7: Up and down electrochemical potentials (dashed lines), their difference (dotted line), the current and density polarizations (solid line) calculated at $x = 0$ as well as magnetoresistance R_m (dashed-dotted line) vs FM polarizations p_f for $E = 1000$ V/cm.

non-magnetic device resistance R_{tr} when $\lambda_{sc} \gg L_s$ and $\lambda_f \gg L_f$ ¹⁸. For a FM/NMS junction we obtain

$$R_m = \frac{L_s}{\sigma_{sc}} \frac{L_s}{\mu_s |E| \tau_s} (1 - \frac{\rho_{\uparrow\downarrow}}{\rho_D}) p_f P(0). \quad (35)$$

Eq. (35) is very interesting: it clearly shows that R_m depends on the intrinsic resistance of the NMS L_s/σ_{sc} , on the ratio between diffusion and drift lengths $L_s/\mu_s|E|\tau_s$ and it emphasizes the dependence of R_m on the spin drag effect. It also shows that the magnetoresistance is proportional to the probability $p_f P(0)$ that a spin crosses the interface without losing its spin polarization, i.e. it preserves its magnetic properties when entering the NMS. Eq. (35) shows that, whichever density regime is considered, the electric field destroys the magnetoresistance.

In Fig. 10 (lower panel inset, curves labelled “1jct”) we plot the ratio between R_m and the total device resistance R_{eq} in respect to the applied field and for $\lambda_{f(sc)} = 10L_{f(sc)}$: such a ratio increases by orders of magnitude with the FM polarization p_f . At $E=0.01$ V/cm, $R_m = 0.28\text{n}\Omega\text{cm}^2$ for $p_f = 0.5$ and $R_m = 8\mu\Omega\text{cm}^2$ for $p_f = 1$.

VII. FM/NMS/FM STRUCTURE

We will now consider the tri-layer structure of Fig. 5b. According to Eq. (10) and to the local charge neutrality constraint Eq. (6), in the NMS the excess spin density components are given by

$$\Delta n_{\uparrow(\downarrow)} = \pm \left[A_0 \exp\left(-\frac{x}{L_d}\right) + A_1 \exp\left(\frac{(x-x_0)}{L_u}\right) \right] \quad (36)$$

where $x_0 > 0$ corresponds to the second interface and the + (-) sign to the \uparrow (\downarrow) component. The chemical

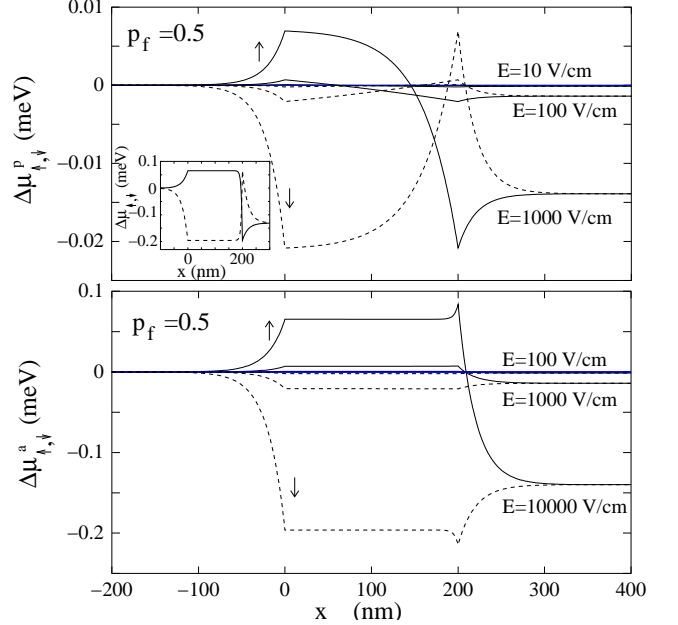


FIG. 8: Upper panel: Up (solid line) and down (dashed line) electrochemical potentials (without the term linear in x) vs x for three different fields (as labelled) and $p_f = 0.5$. The two ferromagnet polarizations are *parallel*. Inset: as in main panel but for $E=10000$ V/cm. Lower panel: As in the upper panel but with *antiparallel* ferromagnet polarizations.

potentials in the three materials are now

$$\begin{pmatrix} \Delta\mu_{\uparrow} \\ \Delta\mu_{\downarrow} \end{pmatrix}_L = e \frac{\vec{j} \cdot \vec{x}}{\sigma_L^f} \begin{pmatrix} 1 \\ 1 \end{pmatrix} + C_L e \vec{j} \cdot \hat{x} \begin{pmatrix} 1/\sigma_{\uparrow,L}^f \\ -1/\sigma_{\downarrow,L}^f \end{pmatrix} \exp\left(\frac{x}{L_L^f}\right) \quad (37)$$

$$\Delta\mu_{\uparrow(\downarrow)} = \pm \frac{D_s e}{\mu_s} (1 - \rho_{\uparrow\downarrow}/\rho_D) P(x) + e \vec{E} \cdot \vec{x} + B_s \quad (38)$$

$$\begin{pmatrix} \Delta\mu_{\uparrow} \\ \Delta\mu_{\downarrow} \end{pmatrix}_R = e \vec{j} \cdot \hat{x} \left(\frac{x}{\sigma_R^f} + B_f \right) \begin{pmatrix} 1 \\ 1 \end{pmatrix} + C_R e \vec{j} \cdot \hat{x} \begin{pmatrix} 1/\sigma_{\uparrow,R}^f \\ -1/\sigma_{\downarrow,R}^f \end{pmatrix} \exp\left(-\frac{(x-x_0)}{L_R^f}\right) \quad (39)$$

where the indices L, R stand for left and right ferromagnets and the + (-) sign in Eq. (38) corresponds to the \uparrow (\downarrow) component. The six constants $\{A_0, A_1, B_{sc}, B_f, C_L, C_R\}$ will be determined by boundary conditions similar to the ones for the single interface, i.e.

$$j_s|_{0^-,x_0^-} = j_s|_{0^+,x_0^+} \quad (40)$$

$$\Delta\mu_{\uparrow}|_{0^-,x_0^-} = \Delta\mu_{\uparrow}|_{0^+,x_0^+} \quad (41)$$

$$\Delta\mu_{\downarrow}|_{0^-,x_0^-} = \Delta\mu_{\downarrow}|_{0^+,x_0^+}. \quad (42)$$

First of all let us consider the spin density and current polarizations. In order to write the expressions for these

quantities we need to derive the expressions for A_0 , A_1 . For general polarizations p_L^f , p_R^f , after some algebra, the expressions for A_0 , A_1 can be written as

$$A_0 = \frac{n}{2} L_u \left(\frac{1}{L_u} - \frac{1}{L_d} \right) \left(p_f^L - \exp\left(-\frac{x_0}{L_u}\right) \frac{d_L^-}{d_R^+} p_f^R \right) \cdot \left[u_L^+ - \exp\left(-x_0 \left(\frac{1}{L_u} + \frac{1}{L_d} \right)\right) u_R^- \frac{d_L^-}{d_R^+} \right]^{-1} \quad (43)$$

$$A_1 = -\frac{n}{2} L_d \left(\frac{1}{L_u} - \frac{1}{L_d} \right) \left(p_f^R - \exp\left(-\frac{x_0}{L_d}\right) \frac{u_R^-}{u_L^+} p_f^L \right) \cdot \left[d_R^+ - \exp\left(-x_0 \left(\frac{1}{L_u} + \frac{1}{L_d} \right)\right) d_L^- \frac{u_R^-}{u_L^+} \right]^{-1}, \quad (44)$$

where

$$d_{R,L}^\pm \equiv 1 \pm G_{R,L} \frac{L_d}{L_{R,L}^f} \quad (45)$$

$$u_{R,L}^\pm \equiv 1 \pm G_{R,L} \frac{L_u}{L_{R,L}^f}, \quad (46)$$

and

$$G_{R,L} \equiv \frac{\sigma_{R,L}^f}{\sigma_{sc}} [1 - (p_{R,L}^f)^2] (1 - \frac{\rho_{\uparrow\downarrow}}{\rho_D}). \quad (47)$$

The spin density and current polarizations are then expressed as

$$P(x) = \frac{2}{n} \left[A_0 \exp\left(-\frac{x}{L_d}\right) + A_1 \exp\left(\frac{(x-x_0)}{L_u}\right) \right] \quad (48)$$

$$\alpha(x) = \frac{2}{n} \left(\frac{1}{L_u} - \frac{1}{L_d} \right)^{-1} \cdot \left[A_0 \exp\left(-\frac{x}{L_d}\right) \frac{1}{L_u} - A_1 \exp\left(\frac{(x-x_0)}{L_u}\right) \frac{1}{L_d} \right] \quad (49)$$

In the interesting case in which $p_L^f = \pm p_R^f = p^f$ (parallel and anti-parallel polarization of the two FM's, which are considered, for the rest, equivalent) the current polarization at the two interfaces becomes:

$$\alpha(0) = \frac{p^f}{d_R^+ u_L^+ - \exp\left(-x_0 \left(\frac{1}{L_u} + \frac{1}{L_d} \right)\right) d_L^- u_R^-} \cdot \left[d_R^+ - \exp\left(-x_0 \left(\frac{1}{L_u} + \frac{1}{L_d} \right)\right) u_R^- \right] \pm \exp\left(-\frac{x_0}{L_u}\right) \frac{G_L}{L_L^f} (L_u + L_d) \quad (50)$$

$$\alpha(x_0) = \frac{\pm p^f}{d_R^+ u_L^+ - \exp\left(-x_0 \left(\frac{1}{L_u} + \frac{1}{L_d} \right)\right) d_L^- u_R^-} \cdot \left[u_L^+ - \exp\left(-x_0 \left(\frac{1}{L_u} + \frac{1}{L_d} \right)\right) d_L^- \right] \pm \exp\left(-\frac{x_0}{L_d}\right) \frac{G_R}{L_R^f} (L_u + L_d), \quad (51)$$

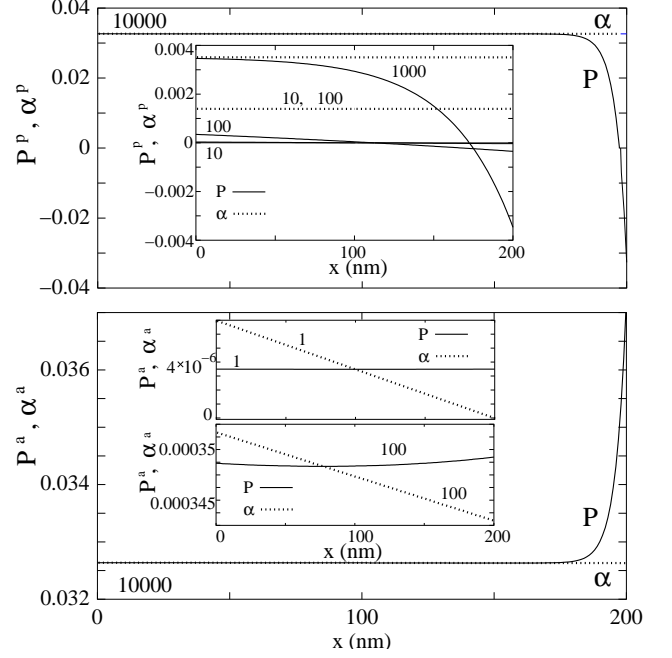


FIG. 9: Upper panel: density (solid line) and current (dot line) polarizations vs x for $E=10000$ V/cm and $p_f = 0.5$. The two ferromagnet polarizations are *parallel*. Inset: as in main panel but for three different fields (as labelled in units of V/cm). Lower panel: density (solid line) and current (dot line) polarizations vs x for $E=10000$ V/cm and $p_f = 0.5$. The two ferromagnet polarizations are *antiparallel*. Upper inset: as in main panel but for $E=1$ V/cm. Lower inset: as in main panel but for $E=100$ V/cm.

where the upper (lower) sign refers to the parallel (antiparallel) configuration.

Finally the expressions for the other constants which appear in the electrochemical potentials are given by

$$B_{sc} = -SnP(0)p_L^f \quad (52)$$

$$B_f = -\frac{x_0}{\sigma_R^f} + \frac{|E|}{|j|} x_0 + \frac{Sn}{e|j|} [p_L^f P(0) - p_R^f P(x_0)] \quad (53)$$

$$C_L = -\frac{Sn}{2} \frac{P(0)}{e|j|} \sigma_L^f (1 - p_L^{f2}) \quad (54)$$

$$C_R = -\frac{Sn}{2} \frac{P(x_0)}{e|j|} \sigma_R^f (1 - p_R^{f2}). \quad (55)$$

In Fig. 8 we plot the behavior of the \uparrow (solid lines) and \downarrow (dashed lines) electrochemical potentials in the trilayer structure for the interesting case in which the NMS width x_0 is much smaller than the diffusion length ($x_0 = L_s/10$). The upper panel shows the electrochemical potentials when a parallel configuration ($p_{fL} = p_{fR} = 0.5$) is considered. The lower panel shows the two junction system when the polarizations of the two FM's are opposite (anti-parallel case, $p_{fL} = -p_{fR} = 0.5$). For both configurations, as the field is increased the potential drop due to the presence of the NMS increases.

We notice immediately that in the parallel case the two spin components of the electrochemical potentials cross. This crossing was predicted to occur in Ref. 1 and is necessary in order to obtain a different potential drop for the \uparrow and \downarrow spin components and hence a finite current polarization even at low electric fields. A clear effect of the electric field enhancement is to “push” the crossing between \uparrow and \downarrow components toward the second interface by increasing the penetration length L_d relative to the first interface and decreasing the upstream penetration length L_u relative to the second interface. This behavior becomes extreme for very high fields (see inset where $E = 10000\text{V/cm}$), where the electrochemical potential components are almost parallel until they suddenly switch before the second interface.

In the antiparallel configuration (lower panel), while the potential drop across the whole structure behaves similarly to the parallel case, the electrochemical potentials do not cross and this behavior destroys the spin current at very low fields¹. The electrochemical potentials present instead a quite distinct feature: for increasing fields a spin accumulation builds up for $x \approx x_0$, just before the second interface, underlining the increasing resistance that spins encounter in crossing this interface when the field (and with it the polarization inside the NMS) increases. This anticipates that in the antiparallel configuration the magnetoresistance is expected to increase with increasing applied electric field.

Fig. 9 presents the behavior of the density (solid lines) and current (dotted line) polarizations as a function of x for both the parallel (upper panel) and the anti-parallel (lower panel) configuration, when the field is increased from the low field regime ($E = 1\text{V/cm}$, $E = 10\text{V/cm}$), to the intermediate ($E = 100\text{V/cm}$), to the high field one ($E = 1000\text{V/cm}$, $E = 10000\text{V/cm}$). The main panel presents the highest field situation. In both configurations, as expected from the behavior in the single junction system, for low to intermediate fields $P(0) < \alpha(0)$, while $P(0) \rightarrow \alpha(0)$ in the high field regime. On the other side, in the parallel configuration, while, due to the choice $x_0 \ll L_s$, $\alpha(x)$ is basically constant even at very low fields, the density polarization $P(x)$ switches sign when the two electrochemical potentials cross. This inversion in the polarization of the spin population unbalance is pushed toward the second interface as the field increases.

The situation is different in the antiparallel case in which, at low to intermediate fields, an almost constant $P(x)$ corresponds to a constant drop of the current polarization $\alpha(x)$ as a function of x . For very low fields ($E = 1\text{V/cm}$), and just before the II junction, it becomes even slightly negative, as could be expected by simply considering the diffusion current at this interface. The drop in $\alpha(x)$ is due to the difficulty in establishing a spin current through the system due to the abrupt decrease of the \uparrow -spin density of states in the second ferromagnet. When the field is increased, the decrement of the current density becomes less drastic while a spin accumulation starts to build up at the second interface (see

lower panel of the inset). In the high field regime finally, it is possible to establish a basically constant spin density current through the device, at the price of building up a strong spin density accumulation just before the second interface (main lower panel).

A. Magnetoresistance

Let us now concentrate on the magnetoresistance. R_{eq} in the FM/NMS/FM structure is given by

$$R_{eq} \equiv -\frac{\Delta\mu(x_0 + \lambda_{f,R}) - \Delta\mu(-\lambda_{f,L})}{e|j|}, \quad (56)$$

where the NMS extends from 0 to x_0 . By writing $\lambda_{f,R(L)} = nL_{fR(L)}$ and using for the electrochemical potentials Eqs. (37),(38) and (39), we obtain

$$\begin{aligned} R_{eq} = & n \left[\frac{L_{fR}}{\sigma_{fR}} + \frac{L_{fL}}{\sigma_{fL}} \right] + \left[\frac{x_0}{\sigma_{sc}} \right] \\ & + \frac{L_s}{\sigma_{sc}} (1 - \exp(-n)) \frac{L_s}{\mu_s |E| \tau_s} \left(1 - \frac{\rho_{\uparrow\downarrow}}{\rho_D} \right) \\ & \cdot [p_{fL}P(0) - p_{fR}P(x_0)] \end{aligned} \quad (57)$$

The first line is clearly the trivial, non-magnetic term. For $n \gg 1$, R_m is given by

$$\begin{aligned} R_m = & \frac{L_s}{\sigma_{sc} \mu_s |E| \tau_s} \left(1 - \frac{\rho_{\uparrow\downarrow}}{\rho_D} \right) \\ & \cdot [p_{fL}P(0) - p_{fR}P(x_0)] \end{aligned} \quad (58)$$

The above equation shows that R_m (i) is proportional to the intrinsic resistance of the paramagnet L_s/σ_{sc} ; (ii) it depends directly on the ratio between the diffusion length $L_s = \sqrt{D_s \tau_s}$ and the drift length $\mu_s |E| \tau_s$, i.e. it tends to diminish with increasing field since the spins will be drifted longer and less resistance occurs (iii) it depends directly on the spin drag which enhances it; (iv) it is proportional to the difference $p_{fL}P(0) - p_{fR}P(x_0) = |p_{fL}P(0)| + |p_{fR}P(x_0)|$. This term can be seen as the probability that magnetic properties remain relevant through the whole structure. It implies that, as long as the products $|p_f P|$ are not vanishing, magnetoresistance is accumulated at the different junctions. (v) In the important case in which $p_L^f = \pm p_R^f = p^f$, the last factor becomes $p_f [P(0) \mp P(x_0)]$: this shows that in the antiparallel case the magnetoresistance is proportional to the sum of the density polarizations just after the first interface and before the second one. This implies that it is enhanced by the spin accumulation at the second interface due to the increasing of the electric field (see Fig. 9).

Fig. 10 illustrates the behavior of the magnetoresistance R_m as a function of the electric field. The main upper panel refers to the parallel configuration. We clearly see that the field decreases the magnetoresistance. The

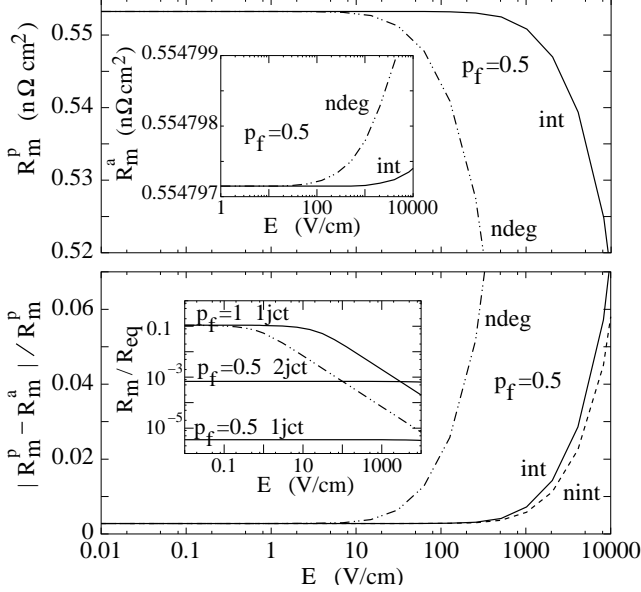


FIG. 10: Upper panel: magnetoresistance R_m for the *parallel* configuration vs electric field for $p_f = 0.5$. Its non-degenerate approximation (dashed-double-dot line) is plotted for comparison. Inset: as for main panel, but for the *antiparallel* configuration. Lower panel: magnetoresistance variation from the parallel to the antiparallel configuration vs electric field for $p_f = 0.5$. Its non-degenerate (dashed-double-dot line) and non-interacting (dashed line) approximations are plotted for comparison. Inset: ratio R_m/R_{eq} vs E for single (1jct) and double junction (2jct, parallel configuration) structures and different FM polarizations (as labelled). For $p_f = 1$ the dashed-double dot line indicates the non-degenerate approximation.

inset shows the corresponding situation for the *antiparallel* case: as anticipated, in this case *the magnetoresistance is increased by the applied electric field*. The lower panel presents the ratio of the difference between the parallel R_m^p and the antiparallel R_m^a magnetoresistances to R_m^p . This relative change in magnetoresistance, responsible for the functioning of spin-valve based devices¹⁷, is increased by the field effect. The non-degenerate and non-interacting approximations are shown for comparison. The inset presents the ratio R_m^p/R_{eq}^p (curve labelled “2jct”) as a function of the applied field. It is interesting to notice that this ratio is about two orders of magnitude higher than the single junction result with the same FM polarization. In systems such that $L_{sc}/\sigma_{sc} \gg L_f/\sigma_f$ in fact, while the magnetoresistance R_m per junction does not change significantly between the single and double junction systems, the non-magnetic component of R_{eq} is mainly determined by the NMS layer length, which strongly decreases in the the tri-layer device. This suggests that, an important requirement for optimizing magnetoresistance-based devices, would be to minimize the NMS layer length.

VIII. COULOMB INTERACTION EFFECTS

Coulomb interactions enter the drift-diffusion equation (Eq. (7)) through the diffusion and mobility constants; in the non-magnetic limit (Eqs. (8) and (9)), through the diffusion constant D_s only, by affecting the spin-stiffness S^7 and generating the spin transresistivity $\rho_{\uparrow,\downarrow}^{5,6,7}$.

First of all, we want to point out that the experimentally important regime $k_B T \lesssim \varepsilon_F$ (see Fig. 1), is the same in which Coulomb interactions between carriers of opposite spin become relevant. In fact for $k_B T \sim \varepsilon_F$ the spin transresistivity reaches its maximum and can become of the same order of the Drude resistivity⁷, while for $k_B T \lesssim \varepsilon_F$ the spin-stiffness displays the maximum deviation from its non-interacting approximation⁷. These two combined effects *reduce* the non-interacting approximation to D_s even by 50%, depending on carrier density and temperature⁷. According to the functional dependence on D_s of the various quantities of interest, Coulomb interaction effects can get amplified, as we will explicitly show for the downstream spin penetration length and for the spin current.

The strong contribution of Coulomb interactions to $L_{u,d}$ values is underlined in the upper panel of Fig. 11 (as well as by the direct comparison between solid and dashed lines in Fig. 3) in which we plot, for GaAs at low temperature, the correction $(L_d^i - L_d^{ni})/L_d^{ni}$ as a function of carrier density and for different fields. Here and in the following i, ni stand for interacting and non-interacting respectively. As the figure shows, the correction can be of the order of 100%, definitely not-negligible when quantitative calculations are required. This correction becomes the largest in the “semiconductor degenerate regime”¹⁵ $e|E|L_s \gg \varepsilon_F \gg k_B T$, when the penetration lengths approach their high field limits $L_d \approx L_s^2 E \mu_s / D_s$, $L_u \approx D_s / (E \mu_s)$, which strongly depend over the diffusion constant. At low densities such a limiting behavior is reached already for $E = 25\text{V/cm}$, while the curve corresponding to $E = 2.5\text{V/cm}$ shows smaller corrections. For higher densities the limiting behavior is reached at larger fields (see the curve corresponding to $E = 250\text{V/cm}$), though the interacting correction remains significant even for fields as low as $E = 25\text{V/cm}$.

The lower panel of Fig. 11 shows the importance of Coulomb corrections in the high field regime, when temperature and carrier density are varied. The largest corrections are present at $T = 1.6\text{K}$ and low densities and are due to the spin stiffness reduction. Even at temperatures as high as room temperature though, Coulomb interactions remain relevant and the correction can be as high as 30%. We underline that in this last case, it is mainly due to the spin Coulomb drag (SCD) effect^{5,7} which enters the diffusion constant through the spin transresistivity (see Eq. (9)). We want to stress that Coulomb interactions modify the behavior of $L_{u,d}$ even qualitatively: as shown for L_d in the lower panel of Fig. 3 ($T = 20, 300\text{K}$), due to Coulomb corrections, the non-

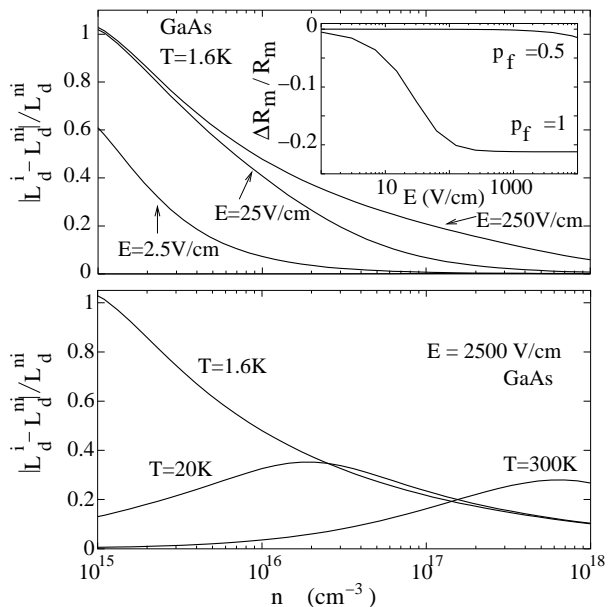


FIG. 11: Upper panel: $|L_d^i - L_d^{ni}|/L_d^{ni}$ vs carrier density for GaAs parameters, $T=1.6\text{K}$ and three different electric fields (as labelled). Inset: $\Delta R_m/R_m \equiv (R_m^i - R_m^{ni})/R_m^{ni}$ vs electric field for $p_f = 0.5$ and $p_f = 1$ (as labelled). Lower panel: $|L_d^i - L_d^{ni}|/L_d^{ni}$ vs carrier density for GaAs parameters, $T=1.6\text{K}$, 20K and 300K (as labelled) and $E=2500\text{V/cm}$.

degenerate limit is approached from above instead than from below when n is decreased. This implies that, even if for high enough temperatures the system can actually enter the non-degenerate regime, the maximum of L_d (the minimum of L_u) is in any case reached *outside* such a regime.

The inset of Fig. 4 shows the Coulomb correction to j_D^d as a function of carrier density and for three different electric fields (as labelled in units of V/cm). Again we notice that the functional dependence of j_D^d on D_s amplifies interaction effects which, depending on the carrier density, are quite substantial.

Let us now consider how Coulomb interactions should affect heterostructures between materials with different magnetic properties. Apart from entering the equations of motion through quantities as the diffusion constant or the penetration lengths, we expect the SCD to play a special role and to affect independently all the quantities related to interface properties. This is due to the very nature of the SCD effect: in fact it tends to relax spin current *opposing relative motion* between up and down spin components, which include opposing all their relative variations connected to injection of a drifting spin unbalance. This picture is confirmed by all our equations related to heterostructures, starting from the expression for the electrochemical potential Eq. (21), in which the spin Coulomb drag enters explicitly through the factor $(1 - \rho_{\uparrow\downarrow}/\rho_D)$. As a consequence, all quantities derived

from this potential as injected spin density, current density, and magnetoresistance, will explicitly display such a factor.

The spin-transresistivity $\rho_{\uparrow\downarrow}$ is a negative quantity, so the factor $(1 - \rho_{\uparrow\downarrow}/\rho_D)$ will *oppose spin injection* in Eqs. (32) and (33), while it will *increase the magnetoresistance* in Eqs. (31) and (58). Since for some systems $\rho_{\uparrow\downarrow} \approx \rho_D^7$, the SCD could actually strongly affect the magnetoresistance. In the calculations here presented though, we have considered only degenerate systems, in which the SCD is usually negligible.

In the inset of Fig. 6, for $E = 1000\text{V/cm}$, we plot both the interacting (solid line) and the non-interacting (dashed line) calculations of the electrochemical potentials: as early discussed, at high fields, interactions increase the spin penetration length L_d in a noticeable way; this correspondingly increases the extension of the polarized region in the NMS.

For all calculations related to heterostructures, we have considered the carrier density $n = 5.2 \times 10^{16}\text{cm}^{-3}$: as can be expected by the upper panel of Fig. 11, the influence of Coulomb interactions should then be not negligible and of the order of 20-25%. This is confirmed by the detailed analysis of the various quantities of interest: in a FM/NMS heterostructure the influence of Coulomb interactions on $\alpha(0)$ and $P(0)$ is of the order of 25% (see inset of Fig. 12). For $E \rightarrow 0$, the ratio $(P_0^i - P_0^{ni})/P_0^{ni} \rightarrow (D_s^i - D_s^{ni})/D_s^{ni}$, while as the field is increased well inside the high field regime, L_u strongly decreases and the Coulomb related term in Eqs. (32) and (33) becomes less important, so that the Coulomb correction starts to decrease. For the same structure, the inset of Fig. 11 presents the Coulomb interaction effects on R_m for increasing electric field and polarization. Here $\Delta R_m/R_m \equiv (R_m^i - R_m^{ni})/R_m^{ni}$. We see that such effects become important as both field and p_f increases.

When we consider a double-junction heterostructure, the effect of Coulomb interactions remains sizeable. In Fig. 12 we plot the interacting (solid line) and non-interacting (dashed line) spin density polarization $P(x)$ across the NMS, both in the parallel (labelled by “p”) and antiparallel (labelled by “a”) configuration for $E = 1000\text{V/cm}$. Again, as for the one-junction case, the interaction correction is of the order of 20-25%. Similarly from the lower panel of Fig. 10 we see that Coulomb interactions at high fields and at the considered density can influence the ratio $(R_m^p - R_m^a)/R_m^p$ by the same amount.

IX. CONCLUSIONS

We have presented a detailed study of spin injection into degenerate semiconductors, analyzing the combined effects of applied electric field, carrier density and Coulomb interactions.

We have clarified the interplay of the different energy scales involved in the problem, proposing an efficient way to understand the regime of the system and

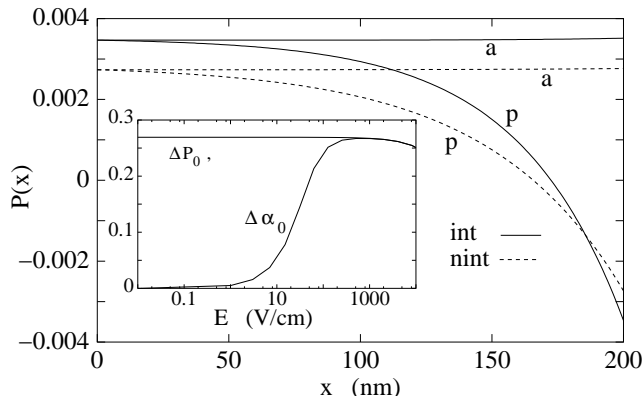


FIG. 12: Double junction system: Density polarization $P(x)$ vs x for the parallel (labelled as “p”) and antiparallel (“a”) configurations (solid line). The non-interacting approximation (dashed line) is plotted as well. Inset: Single junction system: $\Delta P_0 \equiv (P_0^i - P_0^{ni})/P_0^{ni}$ and $\Delta \alpha_0 \equiv (\alpha_0^i - \alpha_0^{ni})/\alpha_0^{ni}$ vs electric field.

estimate the effect of the applied electric field. In particular we have focused on ferromagnet/non-magnetic semiconductor and ferromagnet/non-magnetic semiconductor/ferromagnet structures, carefully comparing the behavior of the relevant quantities (electrochemical potentials, spin density, magnetoresistance...) when the polarization of the second ferromagnet is switched from parallel to antiparallel or its absolute value and the electric field are increased.

We have pointed out, in the anti-parallel case, that the presence of a spin-current through the device is related to the onset of a spin accumulation at the second interface, which in turn increases the device magnetoresistance: at variance with the parallel case, we demonstrate that in the anti-parallel configuration the magnetoresistance can be increased by a strong applied electric field. Additionally we show that this field increases as well the relative change in magnetoresistance $|R_m^p - R_m^a|/R_m^p$, exploited in spin-valve based metal devices¹⁷.

We have proposed a general formalism which includes Coulomb interactions and applies to FM/NMS junctions independently of their carrier density regime. In particular it allows also to study heterostructures in the intermediate regime $\varepsilon \approx k_B T$. “Exact” expressions for the case in which a non-interacting degenerate system is considered have also been provided (see Appendix B).

Our calculations show that, in the experimentally important regime $\varepsilon_f \gtrsim k_B T$, corrections due to Coulomb interactions are relevant. They also demonstrate the importance of carefully identifying the system regime (for example by comparing energy scales as we suggest in Sec.II): non-degenerate approximations in fact, when extended to the wrong regime, can lead to errors of orders of magnitude.

X. ACKNOWLEDGEMENTS

We thank L. W. Molenkamp and G. Schmidt for helpful discussions, G. Vignale for several discussions and very constructive comments and P.E. Mason for carefully reading the manuscript.

APPENDIX A: LIMIT OF THE CHEMICAL POTENTIAL APPROXIMATION

The approximation we proposed for the chemical potential, Eq. (17), can be thought at first sight to be valid only in the low polarization limit $P(x) \ll 1$.

In this appendix we want to estimate the limits of this approximation in the important case of a degenerate system.

In a non-interacting system the Taylor expansion Eq. (15) becomes

$$\mu_\sigma^{chem} = \mu_{0\sigma}^{chem} + \frac{\partial \mu_\sigma^{chem}}{\partial n_\sigma} \Delta n_\sigma + \frac{1}{2} \frac{\partial^2 \mu_\sigma^{chem}}{\partial n_\sigma^2} \Delta n_\sigma^2 + \dots \quad (\text{A1})$$

In a degenerate non-magnetic system, the chemical potential (up to terms of order T^2) is given by

$$\mu_\sigma^{chem} = \varepsilon_{F\sigma} = \frac{\hbar^2}{2m} (6\pi^2 n_\sigma)^{2/3} \quad (\text{A2})$$

Truncating Eq. (A1) up to first order, is equivalent to request

$$\frac{1}{2} \left| \frac{\partial^2 \mu_\sigma^{chem}}{\partial n_\sigma^2} \Delta n_\sigma^2 \right| \ll \left| \frac{\partial \mu_\sigma^{chem}}{\partial n_\sigma} \Delta n_\sigma \right|, \quad (\text{A3})$$

which, using Eq. (A2) becomes

$$P(x) \ll 6. \quad (\text{A4})$$

The above equation implies that, in the important case of a degenerate system, our approximation is valid up to injected polarizations of at least $P(x) \sim 0.5$ ¹⁹. In the special case of a single junction heterostructure it remains valid up to density polarizations of the order of 1. This is shown in Fig. 13, where the effects of the chemical potential approximation discussed at the beginning of Sec.IV are presented for increasing electric field and FM polarization. Fig. 13 compares the results obtained for R_m in the FM/NMS structure using the non-interacting (degenerate) approximation to the chemical potential, with the corresponding “exact” non-interacting degenerate results (see Appendix B). The figure shows that our approximation for the chemical potential gives reasonably small errors (at most of the order of 10%) even for $p_f = 1$. We caution though that this feature cannot be blindly generalized.

Since $|P(x)| \leq p_f$ and the equality corresponds to the high field limit, we have analyzed systems in which p_f satisfies the same limitations found for $P(x)$.

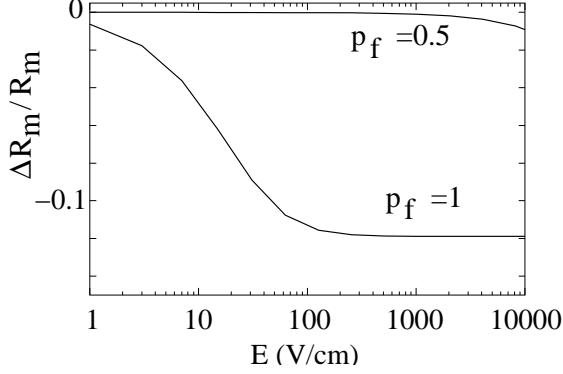


FIG. 13: Correction to the (non-interacting) degenerate approximation for R_m , $\Delta R_m/R_m \equiv (R_m^{exa} - R_m^{deg})/R_m^{deg}$ vs electric field for $p_f = 0.5$ and $p_f = 1$ (as labelled). Here R_m^{exa} corresponds to the (non-interacting) “exact” degenerate calculation.

APPENDIX B: NON-INTERACTING DEGENERATE SYSTEM

If we consider a non-interacting, degenerate NMS, Eq. (18) for the excess electrochemical potential becomes

$$\Delta\mu_\sigma = e\vec{E} \cdot \vec{x} + (\varepsilon_{F\sigma} - \varepsilon_{F\sigma}^0) + B \quad (\text{B1})$$

$$= e\vec{E} \cdot \vec{x} + \varepsilon_{F\sigma}^0 \left[(1 \pm P(x))^{2/3} - 1 \right] + B \quad (\text{B2})$$

where the $+(-)$ sign corresponds to $\sigma = \uparrow (\downarrow)$ and $\varepsilon_{F\sigma}^0$ is the Fermi energy of the unperturbed system.

Applying the conditions (23)-(25), we can now derive the equation for the injected density polarization $P(0)$

$$\begin{aligned} & - \frac{eL_f}{2\varepsilon_{F\sigma}^0} (|j| + |j_D|) \frac{4}{\sigma_f} \frac{1}{1 - p_f^2} P(0) - \{ [1 + P(0)]^{2/3} \\ & - [1 - P(0)]^{2/3} \} + \frac{e|j|L_f}{2\varepsilon_{F\sigma}^0} p_f \frac{4}{\sigma_f} \frac{1}{1 - p_f^2} = 0. \quad (\text{B3}) \end{aligned}$$

Once $P(0)$ is known it is easy to derive all other quantities of interest.

A similar scheme can be applied to the two junction system, where we obtain a system of two implicit equations for the two quantities $P(0)$ and $P(x_0)$, which must be solved self consistently .

- ¹ G. Schmidt, D. Ferrand, L. W. Molenkamp, A.T. Filip and B.J. van Wees, *Phys. Rev. B* **62**, R4790 (2000)
- ² Z.G. Yu and M.E. Flatté, *Phys. Rev. B* **66**, 235302 (2002)
- ³ J.M. Kikkawa and D.D. Awschalom, *Nature* **397**, 139 (1999)
- ⁴ G. Schmidt, C. Gould, P. Grabs, A. M. Lunde, G. Richter, A. Slobodskyy, and L. W. Molenkamp, cond-mat/0206347
- ⁵ I. D’Amico and G. Vignale, *Phys. Rev. B* **62**, 4853 (2000)
- ⁶ I. D’Amico and G. Vignale, *Europhys. Lett.* **55** (2001).
- ⁷ I. D’Amico and G. Vignale, *Phys. Rev. B* **65**, 085109 (2002)
- ⁸ Eqs. (8) and (9) correspond to the limit in which the Drude scattering times for \uparrow and \downarrow spin population are equal; for the more general expressions see Ref. 7.
- ⁹ A well known case is the (Adiabatic) Local Density Approximation in (Time-Dependent) Density Functional Theory, see for example Ref.10.
- ¹⁰ I. D’Amico and G. Vignale, *Phys. Rev. B* **59**, 7876 (1999).
- ¹¹ M.E. Flatté and J.M. Byers, *Phys. Rev. Lett.* **84**, 4220 (2000)
- ¹² L_u, L_d are also known as “diffusion” lengths (see Ref. 2, where their non-interacting approximation was derived). The term “diffusion” is in this case misleading, since for high electric fields $L_{u,d}$ strongly dependent on the drift term. For this reason we prefer to refer to them as “penetration” lengths.
- ¹³ In bulk GaAs, taking as an estimate for low-T τ_s the spin

- decoherence values reported in Ref. 20, and for D_s our calculated value, we find that, $L_s = \sqrt{\tau_s D_s} \approx 2\mu\text{m}$ over the range $10^{16} \text{cm}^{-3} < n < 10^{18} \text{cm}^{-3}$. In (Zn, Be)Se a spin diffusion length of at least $L_s = 2\mu\text{m}$ is considered a reasonable value (L. W. Molenkamp and G. Schmidt, private communication). Our assumption on L_s implies that diffusion constant and spin flip time vary roughly in an opposite way at low temperatures above the metal-insulator transition.
- ¹⁴ P.C. van Son, H. van Kempen, and P. Wyder, *Phys. Rev. Lett.* **58**, 2271 (1987)
- ¹⁵ The interacting and non-interacting systems are defined as having the same diffusion length L_s when no external field is applied.
- ¹⁶ G. Vignale and I. D’Amico, *Solid State Communications* **127**, Issue 12, 829 (2003).
- ¹⁷ G.A. Prinz, *Science* **282**, 1660 (1998)
- ¹⁸ In systems, for which $L_{sc}/\sigma_{sc} \gg L_f/\sigma_f$, the non-magnetic resistance is dominated by the semiconductor component, i.e. $R_{tr} \sim \lambda_{sc}/\sigma_{sc}$.
- ¹⁹ If we apply the same analysis to the non-degenerate case, where $\mu_\sigma^{chem} \sim \ln n_\sigma$, we obtain $P(x) \ll 2$.
- ²⁰ J.J.Kikkawa and D.D. Awschalom, *Phys. Rev. Lett.* **80**, 4313 (1998)